Eur. J. Mech. B - Fluids 20 (2001) 7–24

S0997-7546(00)00093-5/FLA

Trapped vortex optimal control by suction and blowing at the wall

Angelo Iollo, Luca Zannetti *

Dipartimento di Ingegneria Aeronautica e Spaziale, Politecnico di Torino, C.so Duca degli Abruzzi 24, 10129 Torino, Italy

(Received 23 August 1999; revised 3 December 1999; accepted 3 April 2000)

Abstract – The flow due to a vortex trapped in a cavity is considered. The total circulation is constant and such that the Kutta condition is satisfied at the separation point when the vortex is on the equilibrium position S. If the vortex is slightly displaced from S it moves on closed trajectories. By using a classical variational technique, the suction/blowing intensity of the sinks/sources located on the flow boundary is determined so that the vortex is driven back to S. Examples of precomputed control and feed-back control in several flow configurations, including unstable equilibria and in the presence of random perturbations, are given. © 2001 Éditions scientifiques et médicales Elsevier SAS

cavity trapped vortex / precomputed control / feed-back control

1. Introduction

In fluid dynamic applications the designer very often deals with the problem of controlling, reducing and possibly minimizing unsteadiness due either to mechanisms intrinsic to the flow or to unpredictable perturbations present in the environment: “We must always design to achieve orderly airflows and benign vortex shedding from all external surfaces [. . .] Fair everything is the good design motto” [1].

In many cases the unsteadiness is caused by the displacement of large-scale coherent structures present in the flow, such as regions of organized rotational flow that can be, to a first approximation, modeled by point vortices immersed in a potential flow. This approximation is too coarse for a detailed and reliable flow description, but it may provide a simple flow model for a feed-back or precomputed controller.

Examples of flows where the point vortex method (PVM) might be effective are copious; in particular we have in mind applications where the presence of a steady vortex dramatically enhance the performance. Using a potential model, it was shown in [2] that an equilibrium position locus exists for a point vortex trapped by a flat plate at incidence. A similar analysis [3] was conducted for a Joukowsky airfoil obtaining qualitatively the same results.

The lift enhancement due to the trapped vortex is higher by far when the vortex is trapped in the vicinity of the leading edge. However, simplified stability analysis shows that those locations are unstable to small perturbations, i.e., the vortex Hamiltonian has a saddle point, and if the vortex is slightly displaced from its equilibrium position it will not come back. One way to provide a more stable vortex configuration is by forming a cavity in the upper wing surface [4] so that aside from a lift increase, boundary layer effects delay stall at high angle of attack. Experiments show, however, extreme receptivity of the vortex to upstream perturbations. Indeed various instability mechanisms are present in the real flow. Vortex perturbations can be thought as caused by shear-layers instabilities or secondary separations. In particular secondary separations within the cavity can

* Correspondence and reprints.
E-mail address: zannetti@polito.it

be avoided by a cavity design compatible with a cyclic boundary layer [4], as in the case of mountain snow cornices.

Equilibrium configurations alternative to those present on airfoils are not rare; other examples are found in doubly connected domains [5] and in convex corners [6]. In any case, the presence of such vortices characterizes the global features of the flow, and the stability control of such configurations may be important for applications.

On these grounds we explore the effectiveness of simple control devices, namely sources/sinks at the wall, assuming that a point vortex is displaced from its equilibrium position. A similar problem, the motion of a free point vortex near a circular cylinder is considered in [7]. Using two sources of zero mean flow rate at the cylinder wall, the velocity field is modified so that the vortex is put on a stable periodic orbit.

In our case, the geometries of interest mimic more closely the wing cave situation of [4], in order to provide a reference for a forthcoming work on airfoils. The effectiveness of the control law found in a real life application can be evaluated a posteriori with a simulation based on a more sophisticated flow model and the control law computed with the point vortex approximation.

A similar framework was recently proposed in [8] and [9]. Based on a PVM, the authors designed a feedback controller for the stabilization of the two-dimensional unsteady separated flow past a plate perpendicular to the free-stream velocity. The actuator which is reportedly able to stabilize the vortex shedding is a suction point located on the downstream wall. Suction is determined so that the rate of circulation production is zero and there are two steady vortices ensuring the Kutta condition is satisfied at the plate edges. Mathematically the problem of computing suction is formulated as an inverse problem.

In the present study we use a classical variational technique to derive an alternative framework for the design of a nonlinear optimal controller for vortex-dominated flows. We are motivated by the fact that control laws derived from the solution of inverse problems may not be adequate for real life problems. For example it is not evident how to take into account the constraints on the performance of actuators, since the inverse problem may not have a solution for the given constraints.

By formulating the problem as an optimal control problem the control law is designed so that a given functional $\mathcal{L}$ measuring the merit or the cost of a certain solution has a maximum or a minimum respectively. The method to find the actuator control law $g(t)$ so that for any arbitrary $\delta g(t)$ we have $\delta\mathcal{L}(g) = 0$, is based on the Lagrange multipliers technique. Using this technique, see for example [10] for a shape design application, it is possible to determine the Frechét derivative of the functional with respect to $g(t)$ and hence to compute $\delta g(t)$ so that $\delta\mathcal{L}(g)$ is, e.g., positive. Eventually, these iterations converge to the maximum, or to the minimum if we took $\delta g(t)$ so that $\delta\mathcal{L}(g)$ is negative.

2. Potential flow containing a free vortex

The flow model we take into consideration is inspired to Ringleb's study on snow cornices [11] and is the same as used in [12]. Ringleb considered the snow cornices that spontaneously form on mountain crests as natural devices that control flow separation by trapping vortices.

Briefly, he devised the mapping $z = f(\zeta)$:

$$z = \zeta + \frac{\zeta_1^2}{\zeta - \zeta_1}, \tag{1}$$

where $z = x + iy$ is the complex coordinate on the physical z-plane and $\zeta = \xi + i\eta$ that on the transformed ζ-plane.

For a proper choice of the complex parameter ζ_1, equation (1) maps the half plane $\Im(\zeta) > 0$ onto a region of the z-plane bounded by a line that resembles the contour of a snow cornice with a cusp at $z = f(0)$.

The complex potential of a uniform flow over the real axis in the ζ-plane is ascribed to the flow on the corresponding region in the z-plane. A point vortex (and its reflected image) are added to the flow to model the trapped vortex. For a given free-stream velocity q_∞, the circulation κ and position z_0 are determined by enforcing the vortex equilibrium condition $\dot{z}_0 = 0$ and the Kutta condition at the cornice edge. It can be shown that for a proper choice of the parameter ζ_1 a unique stable equilibrium of the vortex is determined.

In [12] the Ringleb model was modified to study the dispersion of scalars in flows characterized by unsteady recirculating regions. For this purpose, the point vortex was slightly displaced from its equilibrium position and let free to move. Since the motion of a free vortex is governed by a one degree of freedom autonomous Hamiltonian system, the displaced vortex moves on a stable closed orbit. On the other hand, the motion of flow particles results in a non-autonomous system. Since the flow domain is non-symmetric under translation or rotation, the system is non-integrable [15]: passive tracers released upstream at constant rate are affected by Lagrangian chaos as they are erratically entrained and detrained by the vortex, generating high concentration regions.

Once the vortex is displaced by its equilibrium locations, the Kutta condition of Ringleb's model is violated. To overcome such incongruity, a blunted edge cornice with large but finite curvature is considered.

Edges with large curvature can still be considered as causing separation: in this case a vortex slightly displaced from its stable equilibrium moves along a small amplitude periodic orbit, and accordingly the detachment point moves, but remains very close to the maximum curvature point. Since the edge is smooth, the flow on the edge is regular without singularities and a Kutta condition can still be considered as fulfilled.

In fact, the flow in the transformed ζ-plane reduces to a vortex pair with the vortices driven on closed orbits. Two oscillating stagnation points – one relevant to the detachment point on the cornice edge, the other to the reattachement point – are present in the flow. The mapping onto the physical z-plane alters the amplitudes of the oscillations, as the lengths in the z-plane are proportional, to first order, to the absolute value of the mapping derivative $|\mathrm{d}z/\mathrm{d}\zeta|$, whose minimum value is at the edge (for a sharp convex edge $\mathrm{d}z/\mathrm{d}\zeta = 0$). This analytical property provides a reasonable extension to the Kutta condition for unsteady flows with negligible vortex shedding and is consistent with the physical behavior of flows with edge induced separations, in which the unsteadiness affects the reattachment quite strongly, but detachment only slightly.

Accordingly, the Ringleb's mapping is modified by adding a further real positive parameter ε:

$$z = \zeta + \frac{\zeta_1^2}{\zeta + i\varepsilon + \zeta_1}. \tag{2}$$

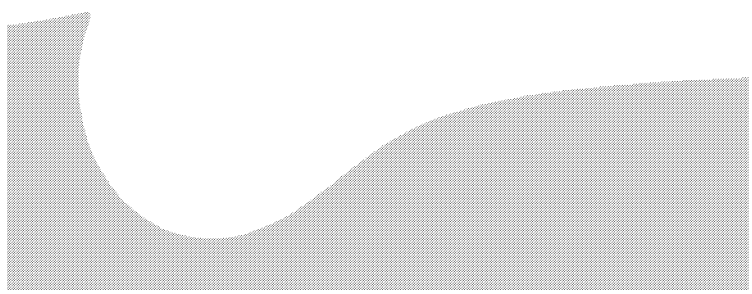

Figure 1. Reference geometry.

Equation (2) is such that the real axis of the ζ-plane is mapped onto the cornice contour, the smaller ε the greater is the curvature of the edge located in $(z)_{\zeta=0}$. For $\varepsilon = 0$ the Ringleb mapping with a sharp cusp is recovered. An example of the geometry generated by this variant of Ringleb's mapping is shown in *figure 1*.

3. Flow and vortex motion

The complex potential of the above depicted flow is expressed by the function:

$$w = \zeta + \frac{\gamma}{2\pi i}\log\left(\frac{\zeta-\zeta_0}{\zeta-\zeta_0^\star}\right), \tag{3}$$

where $\gamma = \kappa/q_\infty$ and * denotes complex conjugation.

From the Lagrangian view point, the motion of flow particles is governed by the Hamiltonian dynamical system:

$$\dot{x} = \frac{\partial\psi}{\partial y}; \qquad \dot{y} = -\frac{\partial\psi}{\partial x} \tag{4}$$

in which the stream function ψ assumes the role of Hamiltonian function and the particle coordinates (x, y) are canonical variables.

Since a vortex does not induce velocity into itself, it moves as a particle in the flow field in which the vortex has been removed:

$$\dot{z}_0^\star = \dot{x}_0 - i\,\dot{y}_0 = \lim_{z\to z_0}\left(\frac{\mathrm{d}w}{\mathrm{d}z} - \frac{\gamma}{2\pi i}\frac{1}{z-z_0}\right). \tag{5}$$

Routh and Kirchoff showed that vortex motions obey Hamiltonian systems as well

$$\dot{x}_0 = \frac{\partial H}{\partial y_0}; \qquad \dot{y}_0 = -\frac{\partial H}{\partial x_0}. \tag{6}$$

The vortex Hamiltonian is not invariant under conformal mapping, but once it is known for a given flow field it can be obtained for any conformally mapped flow field according to Routh's rule [13] which prescribes that if H' is the Hamiltonian pertaining to a free vortex on the complex ζ_0-plane, the Hamiltonian H of the corresponding vortex on the conformally transformed z_0-plane is:

$$H = H' + \frac{\gamma}{4\pi}\log\left|\frac{\mathrm{d}z_0}{\mathrm{d}\zeta_0}\right|. \tag{7}$$

In the present case, it is

$$H' = \eta_0 + \frac{\gamma}{4\pi}\log\eta_0. \tag{8}$$

A vortex trapped in a standing position by the cornice has to satisfy the Kutta condition:

$$\left(\frac{\mathrm{d}w}{\mathrm{d}\zeta}\right)_{\zeta=0} = 0 \tag{9}$$

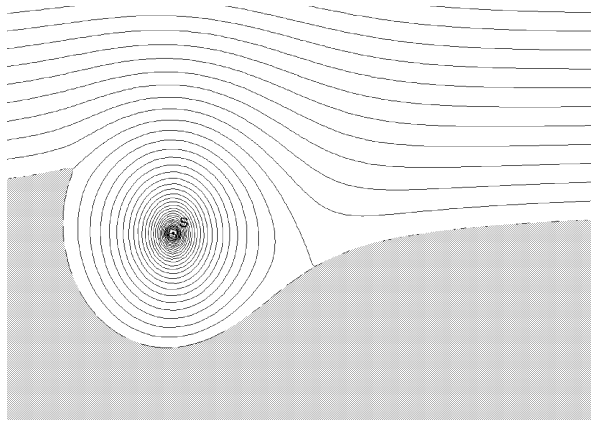

Figure 2. Flow particles streamlines.

and the equilibrium conditions:

$$\dot{x}_0 = \frac{\partial H}{\partial y_0} = 0, \qquad \dot{y}_0 = -\frac{\partial H}{\partial x_0} = 0. \tag{10}$$

The values of the vortex equilibrium position $z_{0\mathrm{eq}}$ and of the ratio of its circulation to the free stream velocity γ are then determined by satisfying equations (9) and (10). In *figure 2* the streamlines corresponding to the vortex located in the equilibrium position are shown.

4. Vortex control

Since H is motion invariant, a vortex trajectory coincides with a level line of H. *Figure 3* shows the level lines of the Hamiltonian relevant to a vortex trapped by the cornice according to equations (9) and (10). The equilibrium position is an elliptic, that is stable, fixed point. Once the vortex is displaced from the equilibrium, it follows a closed periodic orbit. As the flow is unsteady, the stream function becomes dependent on time and the system (4), relative to the flow particles, becomes non-autonomous since the stream function depends on the vortex position. The flow particles exhibit Lagrangian chaos, as discussed in [12], in strong analogy to the Oscillating Vortex Pair (OVP) flow described in [14].

The purpose of the present work is the description of devices capable of driving a displaced vortex back to the appropriate equilibrium (stable or unstable) position.

To this end, we propose to inject or suck air into or from the flow by means of one or several holes in the wall. Such a device can be modeled by adding to the complex potential (3) forcing terms expressing the potential of sources or sinks. For a single source/sink hole, the complex potential flow W is then

$$W = \zeta + \frac{\gamma}{2\pi i}\log\left(\frac{\zeta-\zeta_0}{\zeta-\zeta_0^\star}\right) + \frac{g(t)}{2\pi}\log(\zeta-\xi_g) \tag{11}$$

with ξ_g being the position on the real axis of ζ-plane in which the source/sink is mapped and $g(t)$ the time-dependent source/sink mass flow.

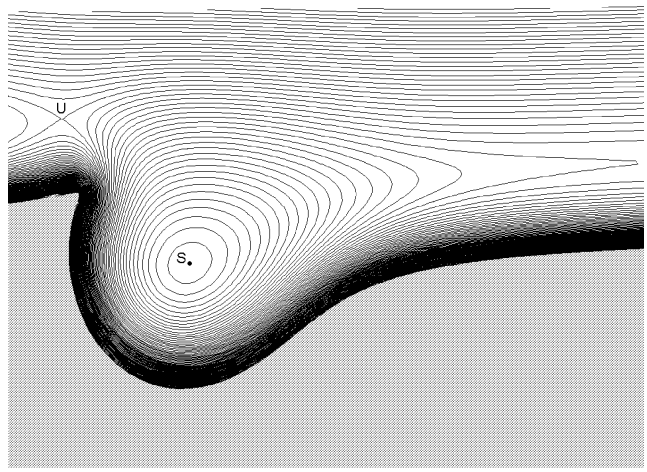

Figure 3. Vortex Hamiltonian. The flow satisfies the Kutta condition when the vortex is in S, the stable equilibrium point. U is the unstable equilibrium point.

The vortex moves according to the time-dependent Hamiltonian system:

$$\dot{x}_0 = \frac{\partial H^g}{\partial y_0}; \qquad \dot{y}_0 = -\frac{\partial H^g}{\partial x_0} \tag{12}$$

with

$$H^g = H + \Im\left[\frac{g(t)}{2\pi}\log(\zeta_0 - \xi_g)\right] \tag{13}$$

and H given by equations (7) and (8).

The control problem that we describe in what follows consists in the determination of the function of time $g(t)$ that in a given time interval $(0{-}T)$ drives a displaced vortex as close as possible back to the equilibrium. That is, we look for the function $g(t)$ that minimizes the quantity $\tilde{\mathcal{L}}$:

$$\tilde{\mathcal{L}} = \frac{1}{2}(\dot{\tilde{x}}_0^2 + \dot{\tilde{y}}_0^2), \tag{14}$$

where $\dot{\tilde{x}}_0$, $\dot{\tilde{y}}_0$ are the components of the vortex velocity at the time $t = T$ with the source/sink device switched off, i.e., $g(t) = 0$ for $t \geqslant T$.

Such a minimum problem is constrained by equations (12). According to the Lagrangian multipliers technique, it can be formulated as an unconstrained problem: instead of the minimum of $\tilde{\mathcal{L}}$ we look for the minimum of the functional $\mathcal{L}$

$$\mathcal{L} = \tilde{\mathcal{L}} + \int_0^T \left[\lambda_1(\dot{x}_0 - H^g_{y_0}) + \lambda_2(\dot{y}_0 + H^g_{x_0})\right] \mathrm{d}t, \tag{15}$$

where λ_1, λ_2 are Lagrangian multipliers to be determined solving an adjoint equation.

Let us consider the function $g(t)$ having a given form and depending on unknown parameters α_i, that is $g = g(t; \alpha_i)$. The first variation of $\mathcal{L}$ with respect to all its arguments is then

$$\delta\mathcal{L} = \left[(H_{x_0}H_{x_0x_0} + H_{y_0}H_{y_0x_0})\delta x_0 + (H_{x_0}H_{x_0y_0} + H_{y_0}H_{y_0y_0})\delta y_0\right]_{t=T}$$

$$+\int_0^T (\lambda_1\delta\dot{x}_0+\lambda_2\delta\dot{y}_0)\,\mathrm{d}t+\int_0^T \left[(-\lambda_1 H^g_{y_0x_0}+\lambda_2 H^g_{x_0x_0})\delta x_0+(-\lambda_1 H^g_{y_0y_0}+\lambda_2 H^g_{x_0y_0})\delta y_0\right]\mathrm{d}t$$
$$+\int_0^T (-\lambda_1 H^g_{y_0g}+\lambda_2 H^g_{x_0g})g_{\alpha_i}\delta\alpha_i\,\mathrm{d}t. \tag{16}$$

To minimize the functional (16) we use a descendent method based on the gradient $\partial\mathcal{L}/\partial\alpha_i$. We have

$$\frac{\partial\mathcal{L}}{\partial\alpha_i}=\int_0^T (-\lambda_1 H^g_{y_0g}+\lambda_2 H^g_{x_0g})g_{\alpha_i}\,\mathrm{d}t \tag{17}$$

once the first three terms on the right-hand side of (16) are set to zero. Integration by parts of the second term yields:

$$\int_0^T (\lambda_1\delta\dot{x}_0+\lambda_2\delta\dot{y}_0)\,\mathrm{d}t=[\lambda_1\delta x_0+\lambda_2\delta y_0]_0^T-\int_0^T (\dot{\lambda}_1\delta x_0+\dot{\lambda}_2\delta y_0)\,\mathrm{d}t. \tag{18}$$

The terms to be set to zero can be then rearranged in the form:

$$[\lambda_1\delta x_0+\lambda_2\delta y_0]_{t=0}=0, \tag{19}$$

$$\left[(\lambda_1+H_{x_0}H_{x_0x_0}+H_{y_0}H_{y_0x_0})\delta x_0\right]_{t=T}=0, \tag{20}$$

$$\left[(\lambda_2+H_{x_0}H_{x_0y_0}+H_{y_0}H_{y_0y_0})\delta y_0\right]_{t=T}=0, \tag{21}$$

$$\int_0^T (-\dot{\lambda}_1-\lambda_1 H^g_{y_0x_0}+\lambda_2 H^g_{x_0x_0})\delta x_0\,\mathrm{d}t=0, \tag{22}$$

$$\int_0^T (-\dot{\lambda}_2-\lambda_1 H^g_{y_0y_0}+\lambda_2 H^g_{x_0y_0})\delta y_0\,\mathrm{d}t=0. \tag{23}$$

Equation (19) is satisfied assuming $\delta x_0=\delta y_0=0$ for $t=0$, whereas equations (22) and (23) provide the adjoint equations for λ_1 and λ_2:

$$\begin{aligned}\frac{\mathrm{d}\lambda_1}{\mathrm{d}\tau}-\lambda_1 H^g_{y_0x_0}+\lambda_2 H^g_{x_0x_0}&=0,\\ \frac{\mathrm{d}\lambda_2}{\mathrm{d}\tau}-\lambda_1 H^g_{y_0y_0}+\lambda_2 H^g_{x_0y_0}&=0\end{aligned} \tag{24}$$

with $\tau=T-t$.

Equations (20) and (21) provide the initial boundary conditions ($\tau=0$) for the adjoint equations (24):

$$\begin{aligned}\lambda_1&=-(H_{x_0}H_{x_0x_0}+H_{y_0}H_{y_0x_0}),\\ \lambda_2&=-(H_{x_0}H_{x_0y_0}+H_{y_0}H_{y_0y_0}).\end{aligned} \tag{25}$$

Once the adjoint equations complete with initial conditions are solved for λ_1 and λ_2, from equation (17) we can compute the gradient of the functional and march toward the extremum.

One way to conceive the minimization algorithm is the following:

(1) Set a time T. At this time the vortex speed will be minimized.
(2) Set an initial position of the vortex.

(3) Assume an initial $g(t)$.
(4) Solve the vortex equations of motion for $t \in [0, T]$.
(5) Solve the adjoint equations for $\tau \in [0, T]$.
(6) Compute the gradient and update $g(t)$.
(7) Continue from step 4 until an extremum requirement is satisfied.

There is a certain freedom allowed in choosing T. Clearly with small T it is not possible to reach the equilibrium point, while it is possible if T is sufficiently large. This occurrence can be exploited for designing two different classes of control laws: the precomputed controller (PCC) and the feed-back controller (FBC).

With large enough T the minimum can be attained, and the law of suction and blowing could be computed for all initial conditions of the vortex using the algorithm presented above. In the following we give computational examples of such a PCC.

On the other hand we know that the model used to compute the control law is a coarse approximation to the true dynamics. Furthermore, there will always be unpredictable disturbances which affect the vortex trajectory. Therefore a more effective controller could be designed if the actual position of what is modeled as the point vortex is taken into account.

This is done by taking a small T and verifying the actual position of the vortex after the application of the control law found by PCC. This kind of 'local' minimization is repeated many times with the vortex updated position as input for the new local minimization. Thus, the effect of unmodeled dynamics and perturbations can be taken into account in the controller design so to achieve an actual FBC by repeated application of many PCC.

4.1. Hamiltonian derivatives

The Hamiltonian H^g can be written as sum of three terms:

$$H^g = H_1 + H_2 + H_3. \tag{26}$$

H_1 is the harmonic part of H^g; it coincides with the stream function of the flow once the vortex and its reflected image across the real axis of ζ-plane are removed:

$$H_1 = \Im(W') \tag{27}$$

with

$$W' = \zeta_0 + \frac{g}{2\pi}\log(\zeta_0 - \xi_g). \tag{28}$$

H_2 is the term due to the reflected image of the vortex:

$$H_2 = \frac{\gamma}{4\pi}\log\eta_0. \tag{29}$$

H_3 is the term due to the Routh rule:

$$H_3 = \frac{\gamma}{4\pi}\log\left|\frac{\mathrm{d}z_0}{\mathrm{d}\zeta_0}\right|. \tag{30}$$

The derivatives ∂H^g are then computed as the sum $\partial H_1 + \partial H_2 + \partial H_3$.

4.1.1. Derivatives ∂H_1, $\partial^2 H_1$

According to the Cauchy condition of analyticity of W', we have:

$$H_{1x_0} = \Im\left(\frac{\mathrm{d}W'}{\mathrm{d}z_0}\right), \qquad H_{1y_0} = \Re\left(\frac{\mathrm{d}W'}{\mathrm{d}z_0}\right); \tag{31}$$

and

$$H_{1x_0x_0} = -H_{1y_0y_0} = \Im\left(\frac{\mathrm{d}^2W'}{\mathrm{d}z^2}\right), \qquad H_{1x_0y_0} = \Re\left(\frac{\mathrm{d}^2W'}{\mathrm{d}z^2}\right). \tag{32}$$

4.1.2. Derivatives ∂H_2, $\partial^2 H_2$

By straight differentiation of (29), we have:

$$H_{2\xi_0} = 0, \qquad H_{2\eta_0} = \frac{\gamma}{4\pi\eta_0}; \tag{33}$$

and

$$H_{2\xi_0\xi_0} = 0, \qquad H_{2\xi_0\eta_0} = 0, \qquad H_{2\eta_0\eta_0} = -\frac{\gamma}{4\pi\eta_0^2}. \tag{34}$$

Then

$$\begin{aligned} H_{2x_0} &= H_{2\xi_0}\xi_{0x_0} + H_{2\eta_0}\eta_{0x_0}, \\ H_{2y_0} &= H_{2\xi_0}\xi_{0y_0} + H_{2\eta_0}\eta_{0y_0} \end{aligned} \tag{35}$$

with

$$\xi_{0x_0} = \eta_{0y_0} = \Re\left(\frac{\mathrm{d}\zeta_0}{\mathrm{d}z_0}\right), \qquad \eta_{0x_0} = -\xi_{0y_0} = \Im\left(\frac{\mathrm{d}\zeta_0}{\mathrm{d}z_0}\right); \tag{36}$$

and

$$\begin{aligned} H_{2x_0x_0} &= H_{2\eta_0\eta_0}\eta_{0x_0}^2 + H_{2\eta_0}\eta_{0x_0x_0}, \\ H_{2y_0y_0} &= H_{2\eta_0\eta_0}\eta_{0y_0}^2 + H_{2\eta_0}\eta_{0y_0y_0}, \\ H_{2x_0y_0} &= H_{2\eta_0\eta_0}\eta_{0x_0}\eta_{0y_0} + H_{2\eta_0}\eta_{0x_0y_0} \end{aligned} \tag{37}$$

with

$$\eta_{0x_0x_0} = -\eta_{0y_0y_0} = \Im\left(\frac{\mathrm{d}^2\zeta_0}{\mathrm{d}z_0^2}\right), \qquad \eta_{0x_0y_0} = \Re\left(\frac{\mathrm{d}^2\zeta_0}{\mathrm{d}z_0^2}\right). \tag{38}$$

4.1.3. Derivatives ∂H_3, $\partial^2 H_3$

Equation (30) can be written as

$$H_3 = -\frac{1}{2}\frac{\gamma}{4\pi}\left[\log\left(\frac{\mathrm{d}\zeta_0}{\mathrm{d}z_0}\right) + \log\left(\frac{\mathrm{d}\zeta_0}{\mathrm{d}z_0}\right)^{\star}\right]. \tag{39}$$

Since

$$\frac{\mathrm{d}}{\mathrm{d}x}\left[\log\left(\frac{\mathrm{d}\zeta_0}{\mathrm{d}z_0}\right)\right] = \frac{\mathrm{d}}{\mathrm{d}z_0}\left[\log\left(\frac{\mathrm{d}\zeta_0}{\mathrm{d}z_0}\right)\right] = -\frac{\frac{\mathrm{d}^2 z_0}{\mathrm{d}\zeta_0^2}}{\left(\frac{\mathrm{d}z_0}{\mathrm{d}\zeta_0}\right)^2},$$
$$\frac{\mathrm{d}}{\mathrm{d}y}\left[\log\left(\frac{\mathrm{d}\zeta_0}{\mathrm{d}z_0}\right)\right] = i\frac{\mathrm{d}}{\mathrm{d}z_0}\left[\log\left(\frac{\mathrm{d}\zeta_0}{\mathrm{d}z_0}\right)\right] = -i\frac{\frac{\mathrm{d}^2 z_0}{\mathrm{d}\zeta_0^2}}{\left(\frac{\mathrm{d}z_0}{\mathrm{d}\zeta_0}\right)^2}, \tag{40}$$

we have

$$H_{3x_0} = \frac{\gamma}{4\pi}\Re\left[\frac{\frac{\mathrm{d}^2 z_0}{\mathrm{d}\zeta_0^2}}{\left(\frac{\mathrm{d}z_0}{\mathrm{d}\zeta_0}\right)^2}\right], \qquad H_{3y_0} = -\frac{\gamma}{4\pi}\Im\left[\frac{\frac{\mathrm{d}^2 z_0}{\mathrm{d}\zeta_0^2}}{\left(\frac{\mathrm{d}z_0}{\mathrm{d}\zeta_0}\right)^2}\right]. \tag{41}$$

Let $F(z_0) = H_{3x_0} - i\,H_{3y_0}$; then

$$H_{3x_0x_0} = -H_{3y_0y_0} = \Re\left(\frac{\mathrm{d}F}{\mathrm{d}z_0}\right), \qquad H_{3x_0y_0} = \Im\left(\frac{\mathrm{d}F}{\mathrm{d}z_0}\right) \tag{42}$$

with

$$\frac{\mathrm{d}F}{\mathrm{d}z_0} = \frac{\frac{\mathrm{d}^3 z_0}{\mathrm{d}\zeta_0^3}\frac{\mathrm{d}z_0}{\mathrm{d}\zeta_0} - 2\left(\frac{\mathrm{d}^2 z_0}{\mathrm{d}\zeta_0^2}\right)^2}{\left(\frac{\mathrm{d}z_0}{\mathrm{d}\zeta_0}\right)^4}. \tag{43}$$

5. Results

The sensitivity of the detachment and reattachment points to changes in the vortex position as well as to suction and blowing at the wall, is presented in *figure 4*. The figure shows the streamlines when a) the source is blowing $g = 1$, b) sucking $g = -1$ and c) when the vortex is displaced from the equilibrium S. The unprimed letters in the figure refer to the unperturbed situation, i.e. $g = 0$ for a) and b) and vortex in S for c). It can be seen that the stagnation point at T does not change remarkably, whereas the one at A is considerably displaced: in case a), for example, it moves inside the field. The vortex shedding from the cornice is therefore going to be very limited, as confirmed by a numerical experiment performed in [12], where it is shown that if a new

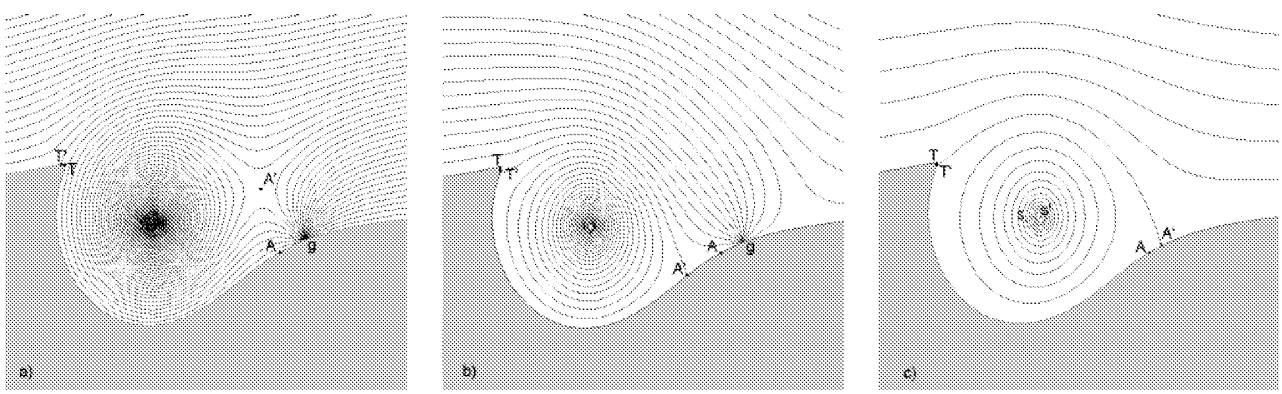

Figure 4. Sensitivity of detachment and reattachment points: (a) blowing; (b) suction; (c) vortex displacement.

point vortex of appropriate vorticity is shed into the field each time the Kutta condition is not satisfied, the total vorticity amount is approximatively constant.

In the following we consider constrained and unconstrained control laws, stable and unstable equilibria, precomputed and feed-back control with and without external perturbations. The numerical integration of the governing and adjoint equations is obtained by a standard fourth-order Runge–Kutta method with constant time step. When $g(t) = 0$ the vortex motion is such that the Hamiltonian is constant. The numerical integration verifies this property to 10 digits.

5.1. Control law

In some of the computational experiments the suction/blowing law $g(t)$ is unconstrained in the sense that the values $g(t_i)$ corresponding to the time discretization are independent variables in the minimization of the functional $\mathcal{L}(g)$. In this case we have

$$\delta\mathcal{L} = \int_0^T \left(-\lambda_1 H^g_{y_0 g} + \lambda_2 H^g_{x_0 g}\right)\delta g(t)\,\mathrm{d}t \tag{44}$$

so that if we take

$$\delta g(t) = -\varrho\left(-\lambda_1 H^g_{y_0 g} + \lambda_2 H^g_{x_0 g}\right), \tag{45}$$

$\varrho > 0$, we have $\delta\mathcal{L} < 0$. The suction law update at optimization step $k+1$ is therefore

$$g^{k+1}(t_i) = g^k(t_i) - \left[-\lambda_1(t_i) H^g_{y_0 g}(t_i) + \lambda_2(t_i) H^g_{x_0 g}(t_i)\right]^k. \tag{46}$$

The study of unconstrained suction laws is of limited practical interest, as the actuator will have certain operative limitations that must be considered. More interesting is to mimic the performance of idealized acoustic sources present on the boundary. In the limit of large wave length or equivalently low frequencies, acoustic multipoles can be modeled by the corresponding singularity of the potential theory.

A monopole is modeled by a source/sink with $g(t) = A\sin(\omega t)$. In particular we tested both amplitude modulation (AM) and frequency modulation (FM) control. For AM control we have

$$\delta g(t) = \delta A(t)\sin(\omega t) \tag{47}$$

and hence

$$\delta A(t) = -\varrho\left(-\lambda_1 H^g_{y_0 g} + \lambda_2 H^g_{x_0 g}\right)\sin(\omega t), \tag{48}$$

whereas for FM control we have

$$\delta g(t) = A\cos(\omega t)\delta\omega(t) \tag{49}$$

so that

$$\delta\omega(t) = -\varrho A\left(-\lambda_1 H^g_{y_0 g} + \lambda_2 H^g_{x_0 g}\right)\cos(\omega t). \tag{50}$$

5.2. Precomputed control

As a first application of PCC we show the results obtained with a single singularity located in the vicinity of the blunted cusp. We take $T = 0.3$ and let P, see *figure 5*, be the initial condition of the vortex. The mass

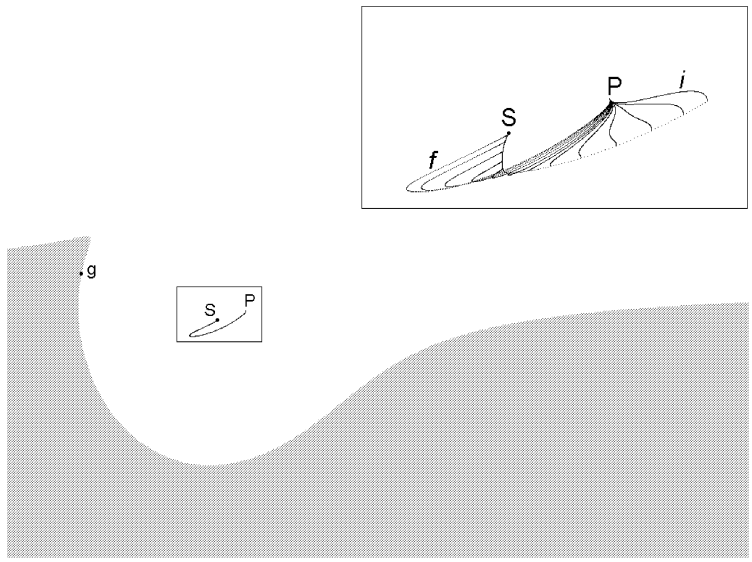

Figure 5. Precomputed control. P is the initial position of the vortex, S the equilibrium and g the position of the source/sink ($\zeta_g = 0.2$ for all cases unless otherwise specified). The trajectories of the vortex during the optimization procedure are evidenced in the zoomed area. The dotted line is the position of the vortex at $t = T$. The letter 'i' denotes the initial trajectory, 'f' the final.

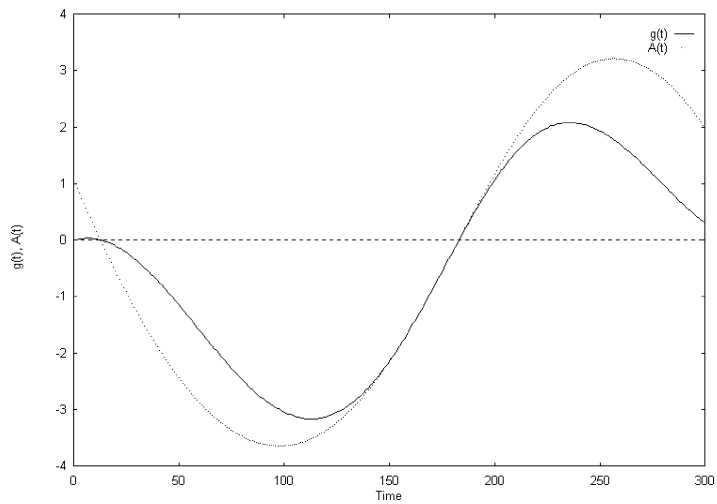

Figure 6. Amplitude modulation with $\omega = 10$, and mass flow for precomputed control.

flow function $g(t)$ is that corresponding to AM control with $\omega = 10$. In all of the following tests the mass flow will be plotted against time step. Each time step corresponds to $\Delta t = 0.001$. The figure shows the trajectories obtained during the optimization procedure and the optimal trajectory. The amplitude modulation and the mass flow pertaining to this case are shown in *figure 6*.

The optimal trajectory does not qualitatively change if we use an unconstrained mass flow function $g(t)$. In *figure 7* the optimal trajectories are presented for two different locations of the actuator ($\zeta_g = 0.2$ and $\zeta_g = 0.6$). In *figure 8* the functions $g(t)$ corresponding to the two cases are plotted.

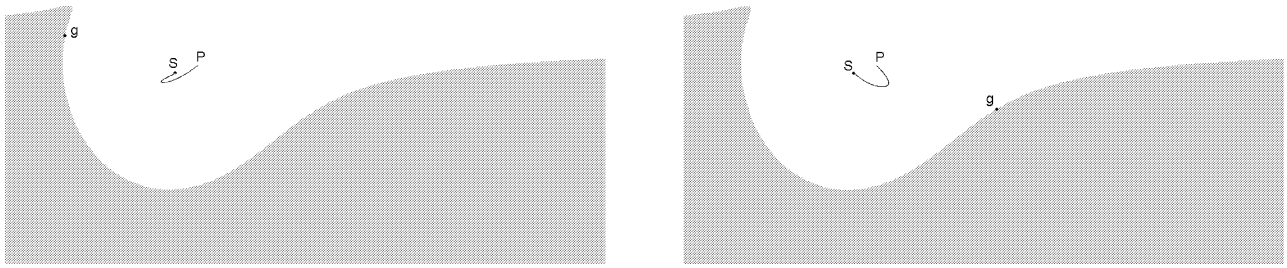

Figure 7. Unconstrained $g(t)$. Left case (i): $\zeta_g = 0.2$; right case (ii): $\zeta_g = 0.6$.

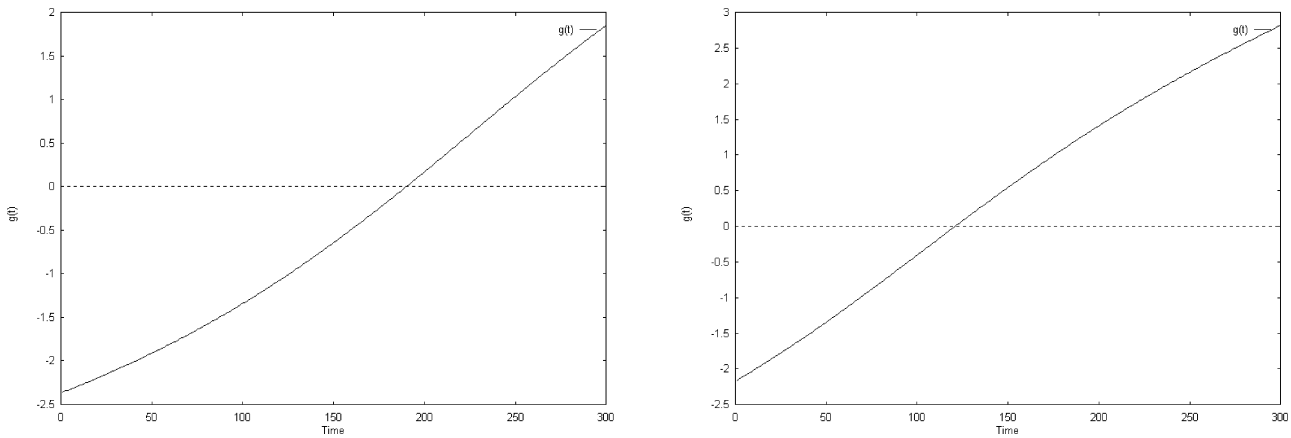

Figure 8. Mass flow; left: case (i), right: case (ii).

For what concerns the FM control we report two cases corresponding to different frequency initializations in the optimization procedure. For both cases $A = 5$.

For large enough T, the minimizing function $g(t)$ is not unique, and an infinite number of control laws can be constructed as suggested by Chernyshenko [16]: let us limit the control law $g(t)$ to a function which is zero on the entire interval $0 < t < T$, except for a very short period $t_1 < t < t_1 + \varepsilon$. During this interval very large values of $g(t)$ have to be used so that vortex velocity not induced by the source/sink will be negligible. Therefore, the vortex will move along the streamlines of the flow induced by a sink/source in the absence of flow at infinity and vortex-induced flow. Among these streamlines there is one passing through S. Hence, the control strategy is simple: put $g(t) = 0$ and wait until the vortex moving along the trajectories of the uncontrolled system crosses that specific trajectory. At this moment turn the control on and move the vortex quickly along that specific streamline and leave it at the equilibrium position. Since in that case the final position depends only on the integral of $g(t)$, the solution is not unique. Therefore, the minimizing function $g(t)$ we obtain depends on the initial guess chosen for $g(t)$ in the descent algorithm. The case in *figures 9* and *10* corresponds to an optimization started with $\omega = 10$, the one in *figures 11* and *12* corresponds to a case initialized with $\omega = 100$.

In order to test the possibility of stabilizing unstable equilibria we set up a case in which the vortex is close to the unstable equilibrium point of *figure 3*. *Figure 13* show that the vortex can attain the unstable equilibrium with the function $g(t)$ of *figure 14*. In this case, however, the Kutta condition is not satisfied at the blunted edge where there would be a release of vorticity which is not taken into account in this model.

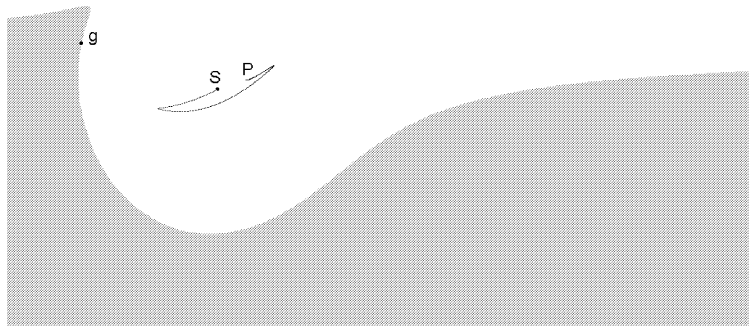

Figure 9. FM control. $\omega = 10$.

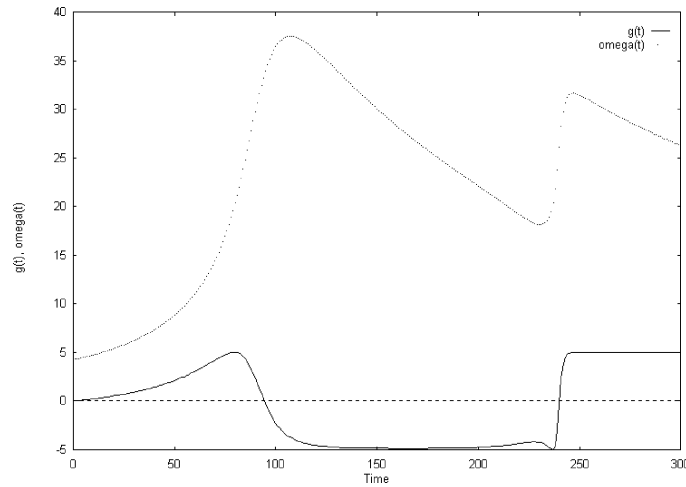

Figure 10. FM control. $\omega = 10$, $A = 5$. Mass flow and frequency modulation.

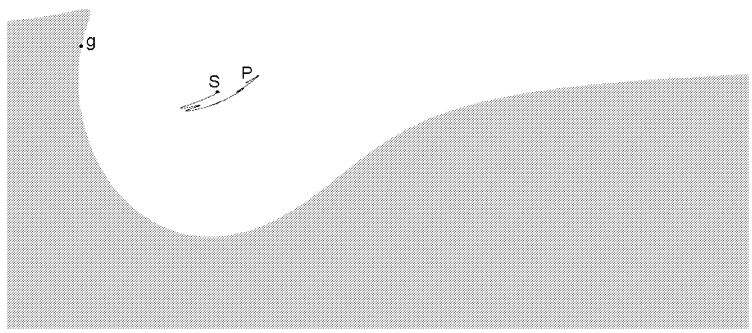

Figure 11. FM control. $\omega = 100$.

5.3. Feed-back control

As explained, the feed-back control is based on many local optimization steps with limited 'horizon' in time, i.e., T is small compared to the time necessary to attain the minimum with the precomputed control. At the end of each local optimization the initial position of the vortex is updated and set to the position at time $t = T$ of

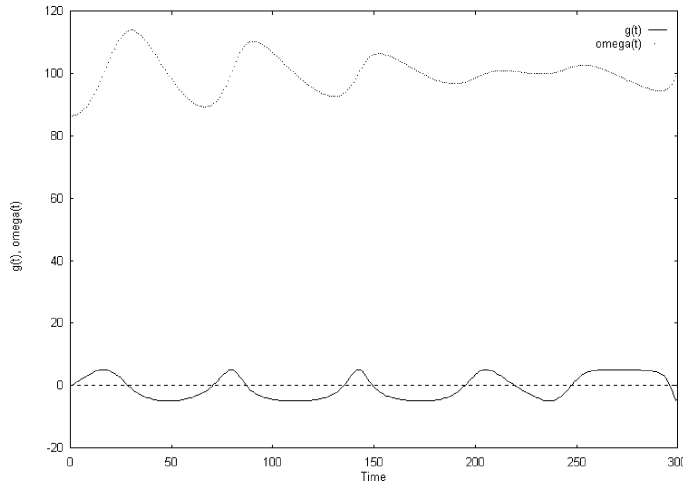

Figure 12. FM control. $\omega = 100$, $A = 5$. Mass flow and frequency modulation.

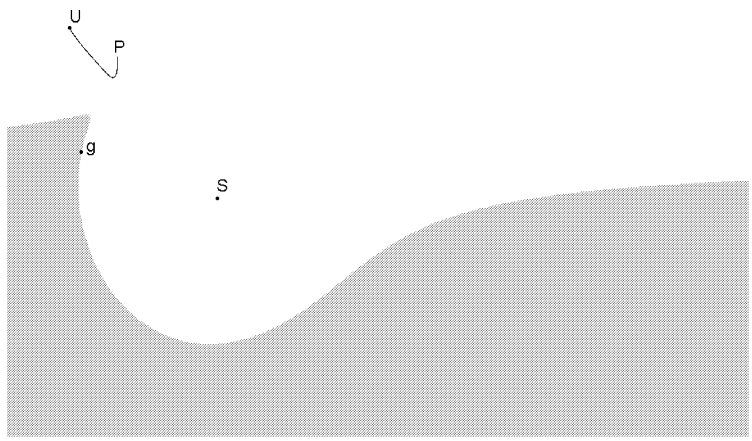

Figure 13. Convergence to unstable equilibrium.

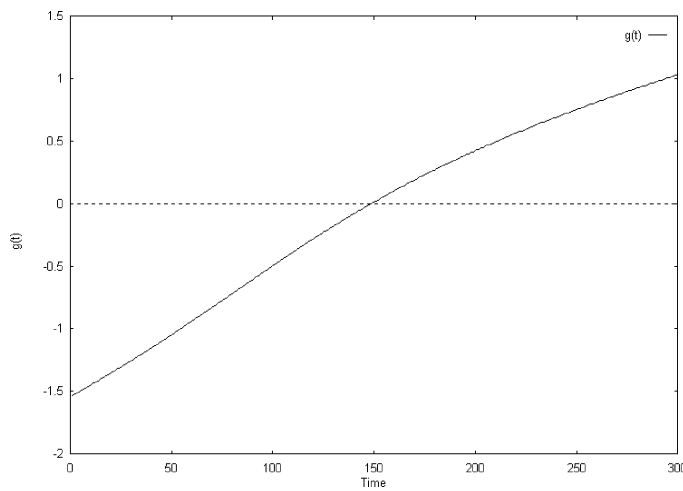

Figure 14. Mass flow for the case of *figure 13*.

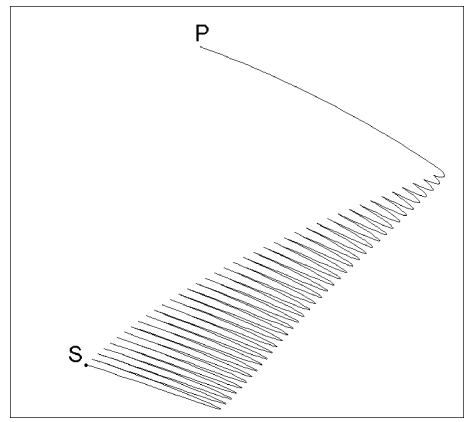

Figure 15. Feed-back control by local optimization. Magnification of the vortex trajectory.

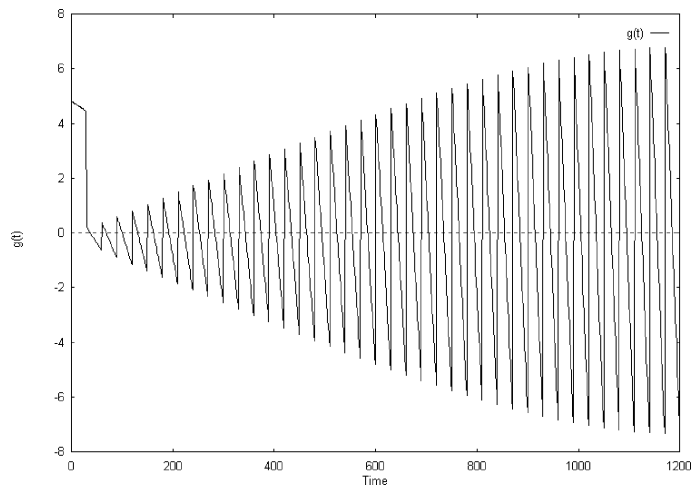

Figure 16. Feed-back control by local optimization. Mass flow.

the previous optimal trajectory. Clearly the vortex speed is discontinuous, as the final speed of the vortex at one step is different from the speed at time $t = 0$ of the next step trajectory.

This implies that the actuator can cope with such an abrupt change of mass flow, which is not a realistic assumption. However, it is possible in principle to have additional constraints on the function $g(t)$ to smooth the discontinuities.

In the test-case we present in *figure 15* another source/sink was added on the cornice in $\zeta_g = 0.6$. The mass flow of such a singularity was taken to be equal in modulus and opposite in sign to that of the first singularity, so that the net mass flow is 0. The potential was modified to include the new singularity, and accordingly the flow and adjoint equations. The function $g(t)$ is plotted in *figure 16*. It is seen that the mass flow is discontinuous. The discontinuities correspond to the local optimizations.

One important issue in control theory is the robustness of the control, i.e., the capability of the control to drive the system in the presence of unmodeled effects due to the actual dynamics. In order to experiment with the robustness of the FBC proposed, we perturb randomly the position of the vortex attained at the end of

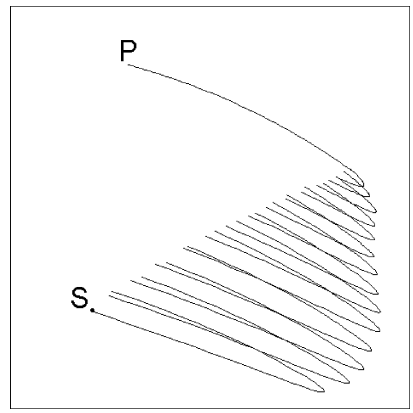

Figure 17. Magnification of the vortex trajectory with random perturbation.

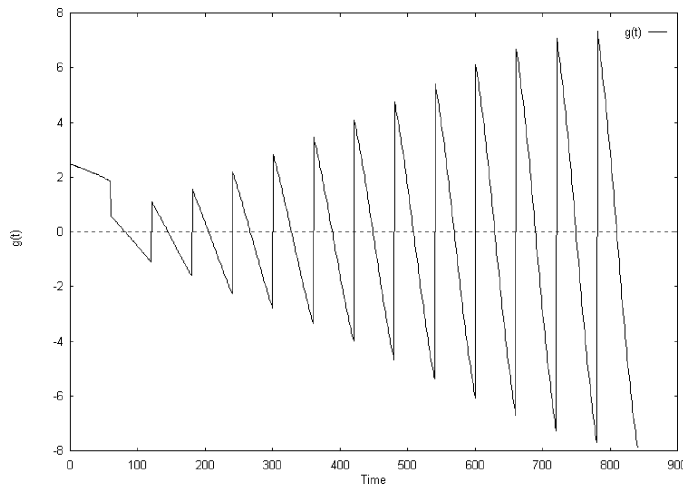

Figure 18. Mass flow of the case in *figure 17*.

the local optimization procedure. Indeed it is still possible to drive the vortex to the equilibrium as shown in *figures 17* and *18*.

6. Discussion and perspectives

In the present paper we have shown the feasibility of two different vortex dynamic control approaches using source/sink singularities on the flow boundaries. The precomputed control is based on a global optimization technique by which the suction and blowing law minimizing the speed of the vortex at time T is found. The main draw back of this approach is that it is not possible to correct the control law for the dynamical effects not modeled in the PVM. It should be remarked that the control strategy proposed in this paper allows the vortex control with only one source, whereas in [7], two sources are necessary. The fact that we use two source with 180 degrees phase shift was dictated by the constraint of zero instantaneous mass injection in the flow, in view of possible practical applications.

The feed-back control makes use of a local minimization procedure after which the actual position of the vortex can be verified and eventually corrected before the next local minimization step. Such a correction implies the presence of a sensor that is able to detect the actual position of the vortex in the flow field, such as that proposed in [8]. The feed-back controller proved to be robust to perturbations in the position of the vortex for reasonable range of parameter excursion. The perturbations simulate either free-stream flow oscillations or position adjustments due to the sensored actual location of the vortex.

However, in this paper we only marginally considered the problem of the optimal location of the actuator. This issue can be relevant for practical applications, as the economic feasibility of the control in terms of the energy involved is influenced by the actuator spatial distribution or topology. With a large mass flow at the boundary singularity the Kutta condition is not satisfied in the present model. The hypothesis of constant circulation can be removed using finer models taking into account the vortex shedding at the cornice edge.

Nevertheless, on the basis of the control examples given in this paper, the perspective seems open to the boundary control of vortex dominated flows by suction/blowing, and in the limit by boundary acoustic disturbances. For example, with FM control it is possible to impose a small mass flow amplitude and yet to control the flow. Indeed the control examples presented must be validated using a more realistic flow simulation, the open issue being the effectiveness in such a context of controllers based on reduced order models.

References

[1] Eldridge A.H., Shuttle performance: lessons learned, NASA CP 2283, Part II, Appendix B, 1983.
[2] Saffman P.G., Sheffield J.S., Flow over a wing with an attached free vortex, Stud. Appl. Math. 57 (1977) 107–117.
[3] Huang M.K., Chow C.Y., Trapping of a free vortex by Joukowski airfoils, AIAA J. 20 (3) (1982) 292–298.
[4] Bunyakin A.V., Chernyshenko S.I., Stepanov G.Yu., High-Reynolds-number Batchelor-model asymptotics of a flow past an airfoil with a vortex trapped in a cavity, J. Fluid Mech. 358 (1998) 283–297.
[5] Elcrat R.E., Hu C., Miller K.G., Equilibrium configurations of point vortices in doubly connected domains, ESAIM Proceeding, Vol. 1, pp. 325–337, 1996; Available at http://www.ematbh.fr/proc/Vol.1/.
[6] Miller G., Stationary vortex configurations, ZAMP 47 (1996) 39–56.
[7] Chernyshenko S.I., Stabilization of trapped vorticies by alternating blowing suction, Phys. Fluids 7 (4) (1995) 802–807.
[8] Cortellezzi L., Leonard A., Doyle J.C., An example of active circulation control of the unsteady separated flow past a semi-infinite plate, J. Fluid Mech. 260 (1994) 127–154.
[9] Cortellezzi L., Nonlinear feedback control of the wake past a plate with a suction point on the downstream wall, J. Fluid Mech. 327 (1996) 303–324.
[10] Iollo A., Salas M., Contribution to the optimal shape design of internal flows with embedded shocks, J. Comput. Phys. 125 (1996) 124–134.
[11] Ringleb F. O., Separation control by trapped vortices, in: Lachmann G.V. (Ed.), Boundary Layer and Flow Control, Vol. 1, Pergamon Press, 1961, pp. 265–294.
[12] Franzese P., Zannetti L., A model of dispersion in the unsteady separated shear flow past complex geometries, E-print: chao-dyn/9907032; available at http://xxx.lanl.gov/.
[13] Routh E.J., Some applications of conjugate functions, P. Lond. Math. Soc. 12 (1881).
[14] Rom-Kedar V., Leonard A., Wiggins S., An analytical study of transport, mixing and chaos in an unsteady vortical flow, J. Fluid Mech. 214 (1990) 347–394.
[15] Zannetti L., Franzese P., The non-integrability of the restricted problem of two vortices in closed domains, Physica D 76 (1994) 99–109.
[16] Chernyshenko S.I., private communication.